UDC 544.015.4

DOI: 10.15372/CSD20180110

Formation and Dissociation of Carbon Dioxide Gas Hydrate in the Pore Space of Al_2O_3

V. G. SMIRNOV[1], A. YU. MANAKOV[2], N. V. SHIKINA[3], Z. R. ISMAGILOV[1,3,4]

[1]*T. F. Gorbachev Kuzbass State Technical University, Kemerovo, Russia*

E-mail: smirnovvg@kuzstu.ru

[2]*Nikolaev Institute of Inorganic Chemistry, SB RAS, Novosibirsk, Russia*

[3]*Boreskov Institute of Catalysis, SB RAS, Novosibirsk, Russia*

[4]*nstitute of Coal Chemistry and Material Science, Federal Research Centre of Coal and Coal Chemistry, SB RAS, Kemerovo, Russia*

(Received December 24, 2017)

Abstract

Decomposition and formation conditions of carbon dioxide hydrate were experimentally determined in porous matrix. As the latter, samples of γ-, θ-, and α-phases of alumina with different porous structure, pore size distribution, and specific surface area were selected. The resulting deviation values of decomposition temperature from the equilibrium curve were compared with a possible diameter of hydrate species computed on the ground of the Gibbs–Thomson equations and known data about the porous structure of the used samples. Comparative analysis of the results of this work and earlier studies of hydrate formation processes in natural coals revealed qualitative differences.

Keywords: hydrates, carbon dioxide, alumina, pores, sorption, phase equilibrium

INTRODUCTION

During the research on the formation and decomposition of gas hydrates of methane and carbon dioxide in different samples of natural coals [1–9], there were acquired experimental and theoretical results demonstrating an opportunity for hydrate formation in natural coals and some peculiarities of their physicochemical behaviour. Along with that, a number of issues remain to be clarified.

Thus, the presence of the threshold value of coal moisture content, with excessing which gas hydrate formation is possible, and also the ability of natural coals to sorb water determine study necessity of probable states, in which water is present [10] in the internal space of natural coal. Furthermore, exploration of the pore structure of coals by different methods gives mixed results [11, 12]. Each grade of natural coal is characterized by different bond energy of sorbed water with coal surface [10] that depends on both organic matter structure and mineral component composition of natural coal. Water sorbed by natural coal is mainly found in a strong connection with the surface and is unable to be involved in hydrate formation. However, with excessing moisture content threshold near the equilibrium curve, hydrate is formed, in other words, the effect of surface interactions on this process is very weak in this case.

© Smirnov V. G., Manakov A. Yu., Shikina N. V., Ismagilov Z. R., 2018

In this regard, the detailed study of gas hydrate formation in the well-described inorganic materials with stable surface properties, clearly defined porous structure, and morphology is required.

Gas hydrates are common in nature [14-17] and are generated from water and gas when exposed to significant mechanical stresses and high gas pressure in the pore space of sedimentary rocks. A coal bed may be their example, in which the formation of hydrates is possible [5–9].

The gas phase of a hydrate-containing bed is most often presented by a mixture of methane, carbon dioxide, nitrogen, and other gases. Their existence requires high (above several MPa) pressure and lowered (in relation to room) temperature. Each hydrate is characterised by its equilibrium curve depending on gas hydrating agent type. Carbon dioxide generates a hydrate of cubic structure I (CS-I) [14]. The elementary cell parameter of the hydrate of this type is 1.2 nm; the latter is formed by 46 water molecules and contains two small and six large cavities that are occupied by guest molecules [14–17]. At 5 °C, carbon dioxide hydrate is stable above 2.3 MPa, and for its stability, the pressure should exceed 3.4 MPa at 8 °C. Hydrate – water – carbon dioxide equilibrium curve is well explored in the lack of extraneous impurities and the effect of surfaces. Approximating the accumulated experimental data, Sloan and Koh [14] provide an analytical expression describing the equilibrium curve of carbon dioxide hydrate. In the 0–11 °C temperature range, it appears as follows:

$$P = \exp\left(44.58 - \frac{10\,246.28}{T}\right) \quad (1)$$

where T is temperature, K; P is pressure, kPa.

Equilibrium conditions of decomposition of gas hydrates may be visibly shifted towards low temperatures (high pressures) due to a change in the surface energy during decreasing particle sizes to 100 nm and less [18–22]. Small hydrate particles are characterised by a high ratio of particle surface area to its volume and hence, by a significant contribution of the surface energy to the total activity of species. The smaller a particle is, the more significant deviation of thermobaric conditions of decomposition from the equilibrium curve is. The size of gas hydrate particles in a porous material is determined by space limitation. Particles of a certain size that are characterised by a specific value of crystallization temperature deviation from the equilibrium curve. Temperature (T_{shift}) digression of hydrate decomposition points from the equilibrium temperature (T_{eq}) may be assessed according to the Gibbs–Thomson equation:

$$\frac{T_{shift}}{T_{eq}} = -\frac{\gamma_h \cos\theta}{\rho_h \Delta H}\left(\frac{f}{d}\right) = -K\frac{f}{d} \quad (2)$$

where γ_h is surface energy at hydrate – host medium boundary; θ is contact angle of hydrate – water – gas interface; ρ_h is hydrate density; ΔH is hydrate decomposition enthalpy; K is coefficient uniting all the above parameters; f is form coefficient, the latter is 4 and 2 for spherical and cylindrical particles, respectively; d is hydrate particle diameter. It can be seen that T_{shift} value is always negative and is determined by the size and shape of hydrate particles. According to [18], for carbon dioxide hydrate in the positive temperature region, $K = 6.2 \cdot 10^{-11}$ m.

Alumina may form several crystal phases [22–29]. The γ-Al_2O_3 phase produced during low-temperature (600 °C) calcination of alumina has the maximum porosity. Above 1000 °C, the θ-Al_2O_3 phase is generated, while higher than 1250 °C – corundum (α-Al_2O_3). Due to the reproducibility and good knowledge of the pore structure, alumina samples may be used as reference pore matrixes with the neutral internal pore surface during studying the formation and decomposition of gas hydrates in the pore space.

The present work experimentally determined the shift from the equilibrium curve of decomposition points and the formation of carbon dioxide hydrate in pore samples. In accordance with the theory based on the Gibbs–Thomson equation, the sizes of the resulting gas hydrate particles were computed. The findings were compared with the pore texture characteristics of the samples under study.

EXPERIMENTAL

Water sorption analysis and low-temperature nitrogen sorption

Earlier, we developed the preparation technique for alumina species of different phase composition and pore structure as high-strength spherical granules to prepare fuel combustion

TABLE 1

Characteristics of alumina samples

Phase composition	Sample	Initial sample fraction size (600 °C), mm	T_{calc}*, °C
γ-Al_2O_3	1γ	0.2–0.4	600
θ-Al_2O_3	2θ	0.2–0.4	1000
α-Al_2O_3	3α	0.2–0.4	1250
γ-Al_2O_3	4γ	0.4–0.8	600
θ-Al_2O_3	5θ	0.4–0.8	1000
α-Al_2O_3	6α	0.4–0.8	1250

* T_{calc} is calcination temperature.

TABLE 2

Characteristics of the porous structure of samples

Parameters	4γ	5θ	6α
A_{BET}, m^2/g	156	88	9
V_{Σ}, cm^3/g	0.48	0.41	0.028
D_{av}, nm	12.2	18.6	12.2
D_{ef}, nm	3.3, 4.7, 11.9	15.5	3.4

catalysts in a fluidized bed [23–25]. This work used three alumina samples: γ-Al_2O_3, θ-Al_2O_3 and α-θ-Al_2O_3 prepared by the liquid moulding method as spherical granules with sizes of 0.2–0.4 and 0.4–0.8 mm [26–29]. Table 1 gives characteristics of the used samples.

Samples 1γ and 4γ, 2θ and 5θ, 3α and 6αhave by pairs identical characteristics of pore structure and differ only by the size. Nitrogen adsorption and desorption isotherms were measured for samples of a size of 0.4–0.8 mm of each phase (4γ, 5θ, 6α) at 77.4 K (−195.75 °C) using an ASAP-2020 devise. With a purpose of the removal of adsorbed gases and water, alumina samples were pre-aged under vacuum conditions at 200 °C for 12 h. Adsorption and desorption measurements were carried out in the range of relative pressures (P/P_0) from 10^{-3} to 0.995. The data were processed by the Brunauer–Emmett–Teller (BET) method with a view to the specific surface area (A_{BET}, m^2/g) and the average pore diameter (D_{av}, nm). The total pore volume (V_{Σ}, cm^3/g) was computed according to the maximum filling of pores. For this series of samples, filling of pores in the range to 170 nm was calculated near point P/P_0 = 0.99 (Table 2). To produce differential pore size distribution (Fig. 1) and the determination of effective pore diameter (D_{ef}, nm), the data of the Barrett–Joyner–Halenda method (BJH) were used. The micropore volume for all samples is negligible (<0.0001 cm^3/g) and is not specified in Table 2.

To construct the water sorption isotherm, the alumina sample was pre-dried in a vacuum furnace at 160 °C during 6 h, and then divided into eight samples, each of which was aged for 50–100 days in a separate desiccator until constant mass. The temperature in the desiccators was constant ((27±2) °C), air humidity therein was set with a saturated salt solution with relative air moisture content above the solution: Na_2CO_3 0.91, KCl 0.84, NaCl 0.75, KI 0.69, $MnCl_2$

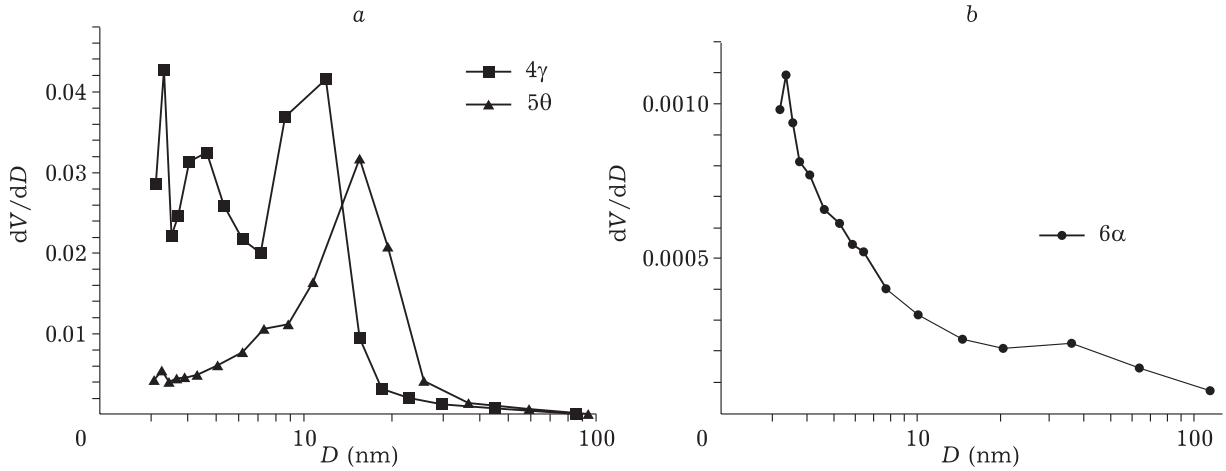

Fig. 1. Pore size distribution (BJH, N_2 desorption) of the studied samples 4γ, 5θ (*a*) and 6α (*b*).

0.56, NaI 0.38, $CaBr_2$ 0.17, and distilled water 1.00. The moisture content of alumina samples was computed as mass change percentage during water saturation. The mass of each sample is about 10 g; measurement precision is 1 mg; the absolute accuracy of determining alumina moisture content was around 0.02 % of sample mass and moisture content ranged from 1 to 50 % of the dry sample weight. Table 3 gives the values of the steady-state moisture content after aging in the atmosphere at a given relative pressure of water vapours (P/P_0) for each of the studied samples of Al_2O_3.

Figure 2 shows the isotherms of water sorption by $A1_2O_3$ samples expressed as the volume of the sorbed water per 1 g of the sorbent. The samples are grouped according to the type of the alumina phase that determine a similar character of the sorption isotherms. For each phase of the alumina samples also the isotherms of nitrogen adsorption and desorption are shown. We suppose that the density of nitrogen in the adsorbed state should be close to that of liquid nitrogen ρ_{liq} = 0.81 g/см^3. Based on this the amount of sorbed nitrogen per unit of the sorbent mass is recalculated into into V_{1iq} – the volume taken by the same amount of nitrogen found in the liquid state, mL/g. The amount of the sorbed water is also measured in the same units. Lines in Fig. 2 connect points of the same type, and they do not mean approximations. It can be seen that for each alumina phase the isotherms of low-temperature nitrogen adsorption are similar by the form and scale to those for water sorption measured at room temperature.

Under similar conditions, samples of the γ-Al_2O_3 phase contain the maximum amount of sorbed water, in case of θ-Al_2O_3 – to a large extent. On the contrary, the amount of sorbed water did not exceed 1 % of sample mass for the α-Al_2O_3 phase, which was an order of magnitude lower than the moisture content of samples of other phases. It is worth noting that for γ-Al_2O_3, a long time was required to reach the steady-state moisture content. Constant wetness for samples placed in the autoclaves with a relative humidity of 0.17–0.84 was reached in about 2 months, and a low mass increase was recorded in probes with the moisture content of 0.91 and 1.00 even after 3 months of ageing.

Examination of hydrate formation in alumina samples

The required moisture content of the samples in experiments for the formation and decomposition of carbon dioxide hydrate was set *via* a method described during constructing water sorption isotherms. The amount of alumina required for loading to the autoclave was dried in a vacuum furnace at 160 °C, and then placed into the desiccator with specified relative air moisture of 0.91 or 0.84. The moisture content of samples was determined according to mass change. It is worth noting that the moisture content of samples may be

TABLE 3

Water sorption by alumina samples

P/P_0	w, %					
	1γ	2θ	3α	4γ	5θ	6α
0.17	4.60	2.64	0.42	4.50	2.06	0.48
0.38	6.12	3.53	0.46	6.23	2.92	0.62
0.56	7.78	4.25	0.51	8.06	3.60	0.70
0.69	10.17	5.07	0.59	10.57	4.30	0.72
0.75	12.02	5.96	0.63	12.33	5.08	0.76
0.84	17.57	8.61	0.73	18.37	6.68	0.84
0.91	23.87	12.89	0.78	25.34	8.00	0.86
1.00	43.99	41.45	4.14	45.30	31.58	3.81

Note. P/P_0 is air moisture content in a desiccator; w is steady sample moisture content, % of dry mass.

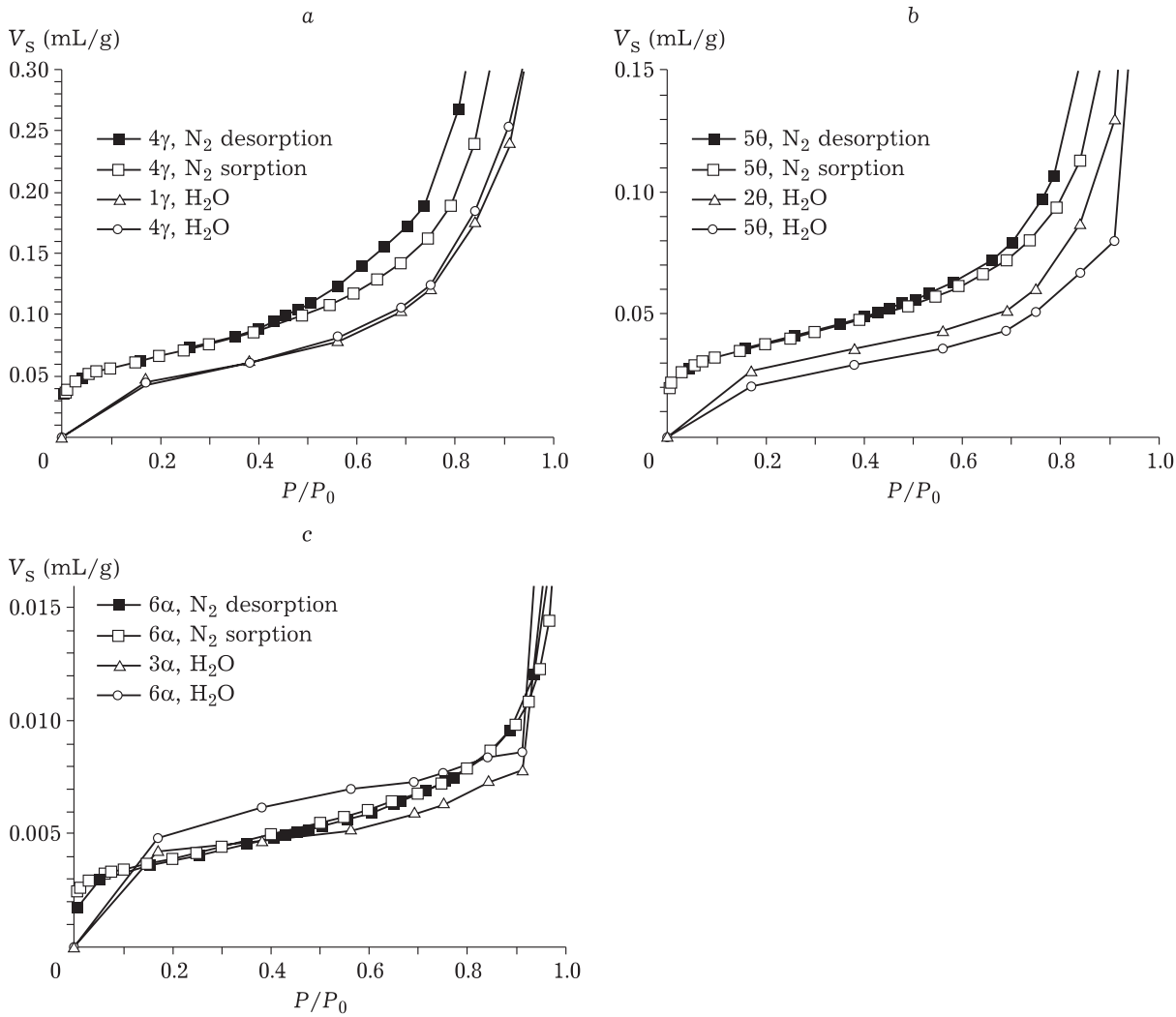

Fig. 2. Low-temperature nitrogen (N_2) sorption isotherms and H_2O sorption isotherms by alumina samples at room temperature: *a* – 4γ, 1γ; *b* – 5θ, 2θ; *c* – 6α, 3α.

somewhat lower than the data of Table 3 that correspond to an exposure of 50–100 days due to exposure time decrease to 20–30 days.

There was an attempt to avoid the sample preparation in the dessicator with a relative moisture content of 1 in order to prevent the formation of dew drops and the filling of contact lenses in the outer surface of neighboring particles with water, as, phase transformations of water in the inner space of pores were investigated. Herewith, the presence of moisture threshold for samples that determine formation opportunity of gas hydrates from sorbed water requires elevated moisture content of the samples. For this reason, desiccators with relative air moisture of 0.84 and 0.91 were selected to prepare experimental samples.

To explore the formation and decomposition of carbon dioxide hydrate in alumina samples, there was used an experimental setup (Fig. 3). The main installation element is a stainless steel cylindrical autoclave (*2*) equipped with an isolation valve (*3*), a pressure transformer (*4*), and a thermocouple (*5*) introduced into the geometrical centre of the autoclave. The autoclave is placed into a programmable cryostat (*1*). Gas pressure and temperature inside the autoclave are measured by means of pressure (*4*) and temperature transformers (*5*, *6*), and also (*6*) the temperature of the coolant washing the outer walls of the autoclave. The data from

the converters are fed to MIT-8 meter (7) and are stored to computer (*8*) memory once in 20 s. Experiments on the formation and decomposition of methane hydrates, carbon dioxide, and natural gas in coal were earlier carried out using a similar facility [1–3, 5, 6].

The prepared Al_2O_3 sample is placed into the autoclave. The free volume of the latter is rinsed with CO_2 to remove the air and free gas pressure is developed. The amount of impurities in carbon dioxide was below 0.01 %. The closed autoclave is found in the freezing chamber of the condenser (−22 °C) at gas pressure inside of the autoclave of 1–2 MPa. These thermobaric conditions correspond to the stable existence of gas hydrates. Herewith, carbon dioxide hydrate is generated in the inner space. The closed autoclave is transferred to a thermostat at a low temperature during the main step of the experiment. Furthermore, a program of linear temperature increase with a rate of 3 K/h from −21 to 12 °C is set. The linear gas pressure increase occurs in the autoclave with the lack of phase transformations. Gas emission during hydrate decomposition is recorded according to the appearance of steps in the pressure change curve. If gas phase volume is known, the amount of CO_2 and H_2O involved in the formation of gas hydrates can be computed. While the step location allows judging of thermobaric conditions, at which decomposition of the generated hydrate occurs.

Calculations of autoclave gas phase volume for each load was performed on the ground of the data regarding the true density of alumina phases: $\rho_\gamma = 3.68$, $\rho_\theta = 3.61$, and $\rho_\alpha = 3.99$ g/cm^3, and also of water density $\rho_{H2O} = 1.00$ g/cm^3. Empty autoclave volume (V_A) was computed from the geometrical sizes of the autoclave and delivery pipes. To compute autoclave volume available for the gas phase (V_g) there was used the following equation:

$$V_g = V_A - m_i(1/\rho_i + w/\rho_{H2O})$$

where i-index indicates one of Al_2O_3 phases; m is loaded alumina mass (per dry condition); w is sample moisture content in this load.

RESULTS AND DISCUSSION

Decomposition of carbon dioxide hydrates in alumina samples

Experiments of the same kind for the decomposition of the developed CO_2 hydrate were carried out for each Al_2O_3 sample. Hydrate decomposition proceeded in the 1.5–2.8 MPa pressure range depending on initial conditions being set. Figure 4 demonstrates typical experimental P–T charts that reflect gas pressure versus temperature during linear heating autoclave

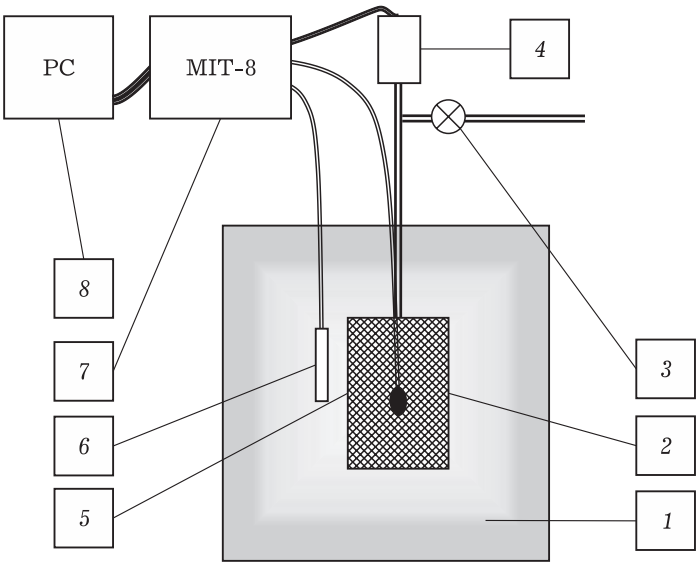

Fig. 3. Experimental plant diagram: *1* – thermostat; *2* – coal and gas autoclave; *3* – gas tap; *4* – pressure transformer; *5*, *6* – temperature converters set inside and outside of the autoclave; *7* – multi-channel MIT-8 measurer; *8* – computer.

with a sample and correspond to experiments carried out with 1γ sample (see Table 1) with the moisture content of 17.71 %. Decomposition of gas hydrates in three experiments (5–7) with gas pressure near a phase transition above 2 MPa was expressed as two steps of the pressure increase of different heights. Designations of these bends (5^1, 5^2, 6^1, 6^2, 7^1, 7^2) are in agreement with the corresponding steps given in Table 4. In two experiments in Fig. 4 (curves *3* and *4*) carried out with the initial pressure of the gas of less than 1.2 MPa, hydrate decomposition occurred in one step, but in a more extended range of temperatures and pressures.

The endothermic effect of carbon dioxide hydrate decomposition is a cause for slowing the growth of temperature inside the autoclave and increasing the temperature difference ($T_{out} - T_{in}$) between the coolant washing the outer walls of the autoclave and the geometric centre of the autoclave, where the thermocouple is installed. Figure 5 demonstrates the measured difference of temperature ($T_{out} - T_{in}$) for each of experimental *P–T* charts given in Fig. 4 depending on the current temperature of the autoclave. The peaks in this dependence correspond to experimental areas where hydrate decomposition takes place. Hydrate decomposition in alumina samples is accompanied by similar thermal effects in all experiments.

The points of the beginning and the end of hydrate decomposition were determined according to each bend in the experimental P–T chart (see Fig. 4). The temperature of the outer walls of the autoclave in experiments with slow linear heating a coolant was close to that of the heat carrier, while the temperature measured in the centre of the autoclave with the thermocouple was by 0.3–0.7 °C lower. Hydrate decomposition begins near the outer walls and ends in the centre of the autoclave. The pressure in the beginning of the bend and the temperature of the coolant washing the outer walls of the autoclave at the given moment are accepted as the initial point of decomposition of hydrates. The pressure in the bend end and the temperature measured in the geometrical centre of the autoclave were accepted as the end point of the range for the decomposition of gas hydrates.

In Fig. 6, the arrows that go from initial to end decomposition points indicate ranges of phase transformations of the hydrate for all experiments performed, and also the code of the sample and moisture content of the latter. Figure 6, *a* (1γ sample) corresponds to *P–T* charts depicted in Fig. 4 and 5. A pair of arrows located along pressure increase curve correspond to experiments with two hydrate decomposition areas. In two experiments with the gas

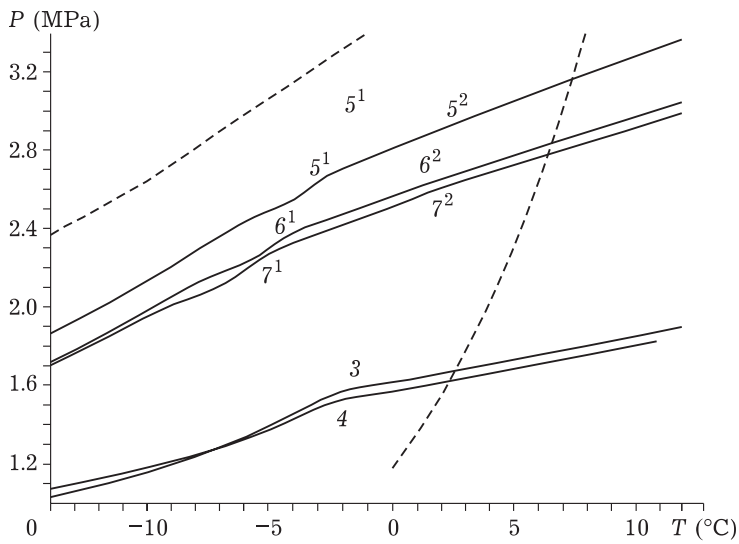

Fig. 4. *P–T* diagrams of experiments with sample 1γ (moisture content of 17.7 %). Numbers indicate decomposition areas of gas hydrates; dot lines – equilibrium curves of liquid carbon dioxide (high) and CO_2 hydrate (right).

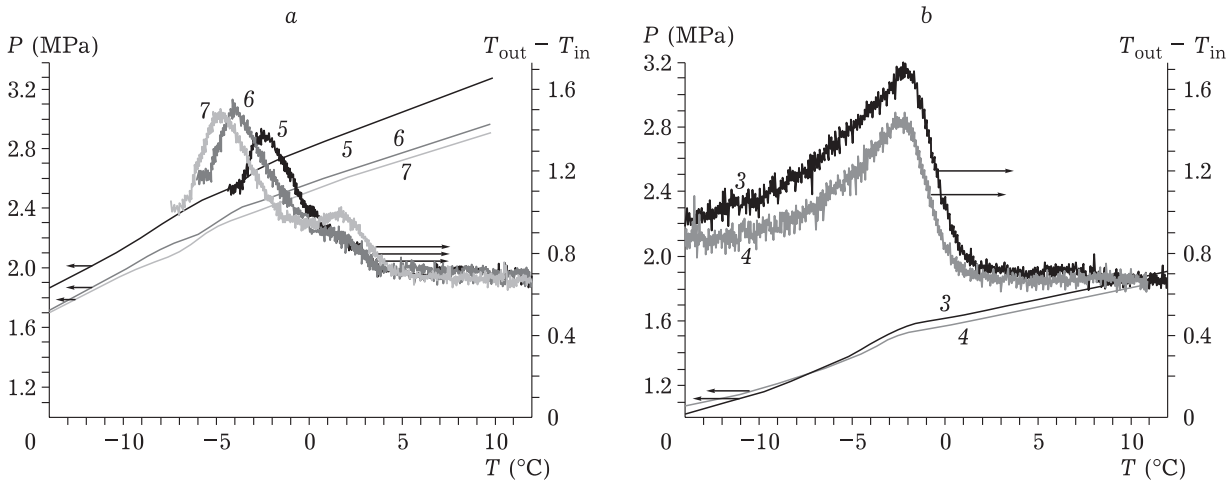

Fig. 5. Curves of the difference in temperatures of heat carrier (T_{out}) and autoclave centre (T_{in}) in experiments with γ-Al_2O_3 samples (moisture content of 17.71 %). Two (*a*) or one (*b*) bends are registered in the *P*–*T* chart for this autoclave load (*a* – at temperatures below −7 °C, boiling of liquid CO_2 occurred, therefore thermal data are not given).

pressure below 2 MPa, hydrate decomposition proceeded in one step, however, the latter was more prolonged. On the contrary, in Fig. 6, *b* (sample 4γ), in samples with gas pressure below 2.2 MPa, there were registered two bends that characterise hydrate decomposition, while in experiments with pressure above 2.4 MPa, there is only one but more prolonged bend. There was a double bend in experiments with 1γ и 4γ, and also 2θ и 5θ samples.

Table 4 gives the description of the experiments. The point with medium temperature (T_m) and medium pressure (P_m) coordinates corresponds to the centre of one of the arrows in Fig. 6 for the range of decomposition of gas hydrates. The T_{shift} value is negative in all cases, in other words, hydrate decomposition proceeds at temperatures below the equilibrium curve (Table 4 gives the absolute value). Here is also the maximum value of the difference between the temperature of the coolant washing the outer walls of the autoclave and the temperature measured in the centre of the autoclave ($T_{out} - T_{in}$) in the range for hydrate decomposition is given.

At each time during the experiment, the amount of CO_2 in gas phase of the autoclave is calculated based on the measured values of gas pressure and temperature inside the autoclave, as well as the calculated free volume of the autoclave available for gas phase. A real gas equation and the Nelson–Obert compressibility chart are used [30]. An increase in the amount of the gas in the autoclave during hydrate decomposition is accepted for the quantity of CO_2 forming the hydrate. Considering that 6.5 water molecules in CO_2 hydrate are accounted for one gas molecule [31], the amount of water forming the hydrate was computed. For the convenience of comparing the results, the amount of water in the hydrate (w_h, see Table 4) was recalculated as the percentage of the mass of dry alumina sample in each load.

Effect of the shape and size of hydrate particles on its decomposition temperature shift

As demonstrated earlier [18], the experimental data for decomposition temperatures of gas hydrates produced in limiting SiO_2 pores may be interpreted using equations (2). It was found [18] that in the case of close to 100 % filling of the pore space with water, to describe the influence of the size effect on decomposition temperature of the hydrate present in the pores, it was desirable to use D_m pore size (see Table 2), in other words, the maximum in the pore size distribution curve. Experimental points [18] may fall into the range limited by curves for *f* of 2 (cylindrical particles correspond to hydrate particles intensely intergrown into silica gel pore space, moreover, the size of these particles is significantly greater in one of the trends) and of 4 (spherical species conform to hydrate ones, close to nanoscale). The appearance of double effects due to the presence of several particle populations

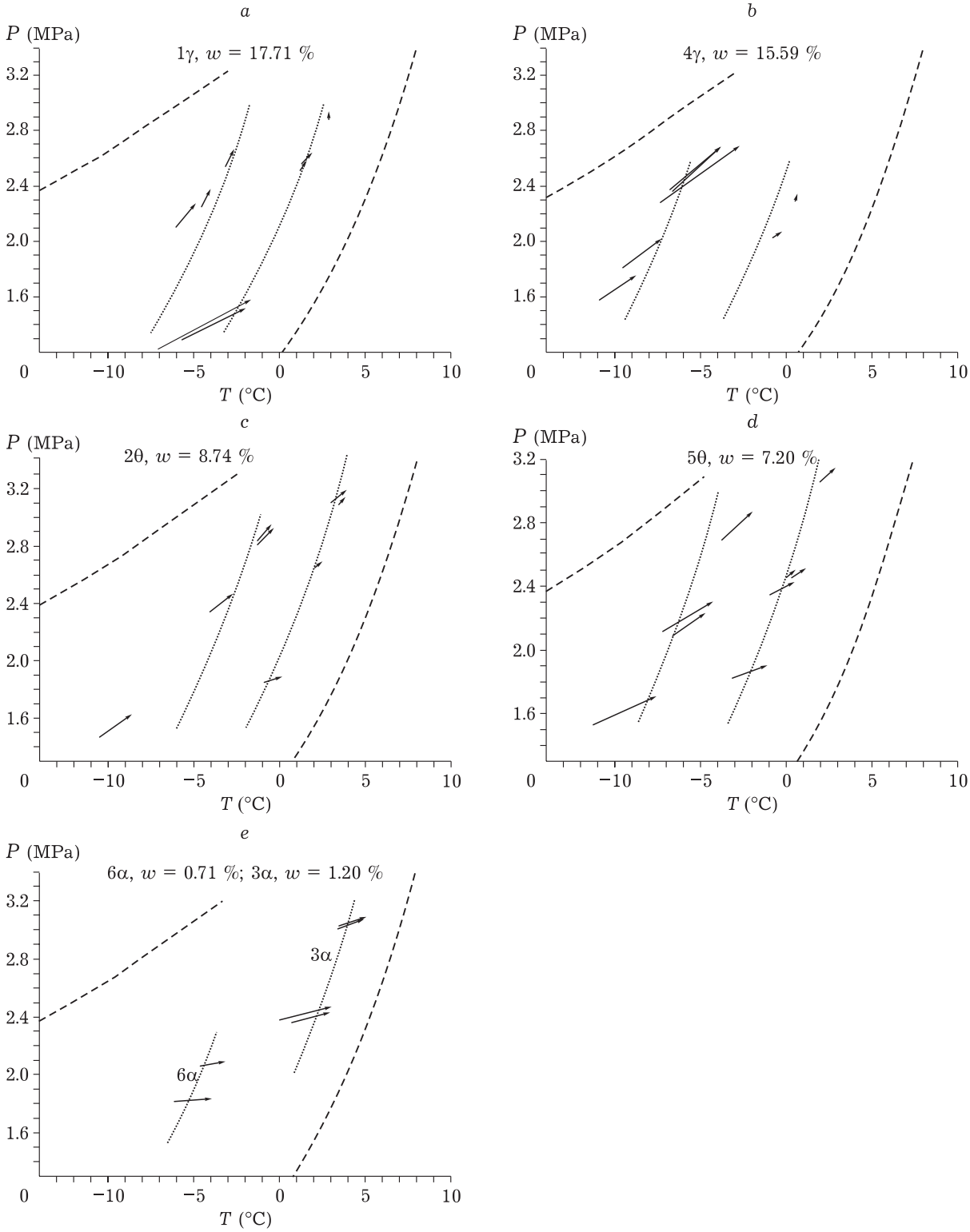

Fig. 6. Charts of decomposition of carbon dioxide hydrate (arrows) in alumina samples (*a*–*f*). See Table 1 for codes of the samples. Dash lines indicate equilibrium curves of liquid and gaseous CO_2 (high) and CO_2 hydrate, liquid water and gaseous CO_2 (right). Points identify decomposition lines of hydrate species of limited sizes.

TABLE 4

Data on decomposition of CO_2 hydrates in pores of the studied alumina samples

Number	Sample	Transition type	w_h, %	T_m, °C	P_m, MPa	T_{shift}, °C	$T_{out} - T_{in}$, °C
			1γ, w=17.71%, P/P_0 = 0.84				
3	1γ	Sole	1.45	−4.3	1.41	7.6	1.06
4	1γ	Same	0.90	−3.9	1.41	6.4	0.81
5^1	1γ	First	0.36	−2.9	2.60	8.9	0.74
5^2	1γ	Second	0.04	2.9	2.93	3.9	0.25
6^1	1γ	First	0.36	−4.3	2.32	9.3	0.88
6^2	1γ	Second	0.07	1.8	2.62	4.6	0.25
7^1	1γ	First	0.36	−5.5	2.20	10.3	0.84
7^2	1γ	Second	0.09	1.4	2.56	4.5	0.36
			2θ, w=8.13%, P/P_0 = 0.82				
8	2θ	Sole	0.06	−2.9	2.55	9.0	0.18
9	2θ	Same	0.40	−3.5	2.74	10.7	0.42
			2θ, w=8.74%, P/P_0 = 0.84				
12^1	2θ	First	0.49	−0.9	2.89	8.0	0.44
12^2	2θ	Second	0.03	3.5	3.15	4.5	0.11
13^1	2θ	First	0.57	−0.9	2.87	7.9	0.43
13^2	2θ	Second	0.03	3.6	3.12	4.0	0.09
14^1	2θ	First	0.16	−3.4	2.41	9.3	0.46
14^2	2θ	Second	0.05	2.2	2.67	4.0	0.11
15^1	2θ	First	0.25	−9.6	1.55	12.4	0.43
15^2	2θ	Second	0.05	−0.5	1.87	4.2	0.11
			3α, w =1.21 %, P/P_0 = 0.91				
16	3α	Sole	0.09	4.3	3.06	3.7	0.12
17	3α	Same	0.06	4.1	3.04	3.7	0.12
18	3α	Same	0.13	1.5	2.43	5.2	0.12
19	3α	Same	0.13	1.9	2.40	4.5	0.12
			4γ, w=15.59%, P/P_0 = 0.80				
21	4γ	Sole	1.01	−5.3	2.57	12.2	0.52
22	4γ	Same	0.64	−5.3	2.56	12.1	0.63
23	4γ	Same	0.92	−5.1	2.53	12.8	0.59
24^1	4γ	First	0.55	−8.4	1.98	13.0	0.54
24^2	4γ	Second	0.02	0.7	2.38	4.5	0.06
25^1	4γ	First	0.64	−9.8	1.74	13.5	0.52
25^2	4γ	Second	0.02	−0.5	2.11	5.0	0.07
			5θ, w=7.20%, P/P_0 = 0.87				
26^1	5θ	First	0.72	−2.8	2.78	9.9	0.45
26^2	5θ	Second	0.09	2.5	3.10	5.0	0.14
27^1	5θ	First	0.54	−5.6	2.22	11.3	0.46
27^2	5θ	Second	0.13	0.4	2.48	5.4	0.11
28^1	5θ	First	0.36	−5.7	2.21	11.6	0.38
28^2	5θ	Second	0.13	0.8	2.49	5.7	0.08
29^1	5θ	First	0.48	−5.6	2.16	10.9	0.41
29^2	5θ	Second	0.05	−0.2	2.39	6.1	0.12
30^1	5θ	First	0.45	−9.4	1.62	13.3	0.38
30^2	5θ	Second	0.14	−2.2	1.86	6.5	0.13
			6α, w=0.71%, P/P_0 = 0.63				
31	6α	Sole	0.13	−3.9	2.08	8.7	0.05
32	6α	Same	0.13	−5.1	1.83	9.4	0.05

Note. w_h is amount of water involved in hydrate formation; T_m, P_m are temperature and pressure in the middle of a phase transition, respectively, computed as mean in the beginning and at the end of phase transitions; T_{shift} is shift value of hydrate decomposition temperature in relation to equilibriums determined as temperature difference in the initial point of phase transitions at the same gas pressure (negative in all cases); $T_{out} - T_{in}$ are maximum temperature difference for the experiment in the thermostat bath and geometrical autoclave centre.

different in the shape and/or size is feasible.

However, the formal calculation of T_{shift} values according to the method of [18] for γ-, θ-and α-Al_2O_3 samples (see Table 2) gives shifts of 3.1–6.2, 2.4–4.7, and 14.2–28.4 °C, respectively (the first temperature was computed at $f = 2$, the second one – at $f = 4$). It can be seen (see Table 4) that the experimentally measured T_{shift} values are significantly different from the calculated ones, that is the average pore size for γ- and θ-Al_2O_3 samples is less than the corresponding pore size distribution maximum (see Fig. 1 and Table 2). In the case of the α-Al_2O_3 sample, the situation is exactly the opposite.

As it follows from the data of Table 4, only a small portion (below 10 %) of water sorbed by alumina samples is involved in the formation of carbon dioxide hydrate. The amount of water sufficient for hydrate formation may be present in pores the diameter of which not necessarily corresponds to the maximum in the pore size distribution curve.

It is known that water adsorption in sorbents similar to the selected alumina proceeds in two steps. At first, the hydrophilic surface of the sorbent is covered with a water film with 0.5–1.0 nm thickness and micropores filling occurs (this water can be tentatively called tightly bound). A fast increase in the initial area of a sorption isotherm corresponds to this process (see Fig. 2). Hereafter, with increasing the partial pressure of water vapours, filling mesopores with an increasingly greater size takes place. As demonstrated by the comparison of the data of Table 4 and Fig. 2, only a portion of water sorbed during the second step turns into the hydrate. Apparently, the hydrate formation reaction in the pore space is mainly carried out at the borderlines of the gas – water contact. Herewith, only a part of the water contained in the sample is converted into hydrate, and the remaining free water is buried under the hydrate crust or is present in thin pores and layers, the size of which is smaller than the minimum possible dimension of hydrate particles.

In the case of partial filling of pores, the size of hydrate particles is rather close to the diameter of the curvature of the capillary water surface. The condition of the mechanical equilibrium of the water domains in the pore space requires that all water – gas contacts would be limited to menisci of the same curvature. Curvature diameter (D_c) is determined by the partial pressure of water vapours, the equilibrium moisture content of the sample and can be computed according to the Kelvin equation:

$$D_c = -\frac{4\gamma_l \cos\theta}{\rho_l RT \ln\left(P/P_0\right)} \quad (3)$$

where R, T are universal gas constant and temperature; ρ_l is liquid water density; γ_l is surface tension at the liquid – vapor boundary; θ is contact angle. To carry out calculations according to formula (3), similarly to [18, 22], it should be accepted that $\gamma_l = 0.03$ J/m^2, and $\cos\theta = 1$. The relative humidity (P/P_0) value corresponds to air moisture content (see Table 3 and Fig. 2), at which the wetness of the sample used in the experiments is reached.

An array of data obtained in this paper (see Table 4) is comparable with the results of [18]: hydrate decomposition in all cases is shifted towards low temperatures by 4–14 °C. For one part of the experiments, there was one step of hydrate decomposition, for the other – two and (possibly) more. For single-type samples, T_{shift} values in case of single effects fall within the range limited by T_{shift} values for double effects. The T_{shift} values for double effects differ almost twice in most cases.

Suppose mid-temperature intervals of two steps of hydrate decomposition correspond to the situations with $f = 2$ and $f = 4$ (equation (2)), and the middle of the only stage of decomposition corresponds to the middle line between the curves with $f = 2$ and $f = 4$. In this case, the data of Table 4 allow fairly reliably assessing the typical size of hydrate particles and the size of limiting pores, in which hydrate particles are formed in the studied samples. Table 5 gives the sizes of hydrate particles selected on the ground of equation (2), which best approximate the experimental results of Table 4. In Fig. 6, the points indicate the calculated equilibrium lines of cylindrical $f = 2$ and spherical $f = 4$ hydrate particles with a diameter (D_h) specified in Table 5.

Considering the presence of a water film between the hydrate particle and pore wall, films of water that does not turn into the hydrate, the size of pores accommodating hydrate species

TABLE 5

Assessment results of the diameter of hydrate species (D_h) generated in alumina pores

Sample	D_h, nm	D_c, nm	D_m, nm
1γ, w=17.71 мас.%, P/P_0=0.84	8.0	14.0	12.0
2θ, w=8.13 мас.%, P/P_0=0.82	7.5	12.0	16.0
2θ, w=8.74 мас.%, P/P_0=0.84	8.5	14.0	16.0
3α, w=1.21 мас.%, P/P_0=0.91	11.0	25.0	3.4
4γ, w=15.59 мас.%, P/P_0=0.80	6.0	11.0	12.0
5θ, w=7.20 мас.%, P/P_0=0.87	6.2	17.0	16.0
6α, w=0.71 мас.%, P/P_0=0.63	8.0	5.1	3.4

Note. D_c, is curvature diameter of the surface of water species at the gas – capillary moisture interface; D_m is maximum position in the pore size distribution curve.

should be somewhat (~1 nm) higher than the dimension of the latter. The cosine of the edge angle was taken equal to one, in this case, D_c diameter will be equal to that of gas hydrate particles (D_h), however, in reality, $\cos\theta < 1$, hence, $D_h < D_c$. This ratio, with one exception, is observed in Table 5. In almost all cases, the size of hydrate particles increases with a rise in the equilibrium value of air humidity, at which the sample was saturated with water.

The emergence of two particle types (of spherical and cylindrical shape) in pores of the alumina sample is quite explainable. Even if sample pores are cylindrical, their filling begins from the blind end, on which the first drop of water with a shape close to spherical is formed. Overwinds, shape inhomogeneities, and bends of cylindrical pores, and also commissures of pores of different sizes and orientations are filled at the first stage. In all these cases, there are areas of capillary condensation with approximately equal dimensions in all directions, *i.e.* water droplets of almost spherical shapes (f = 4). At subsequent sorption stages, the cylindrical channels are completely filled, and gas hydrate particles of cylindrical shape (f = 2) are formed in pores of the same diameters. Thus, with the same surface curvature of capillary water, hydrate particles that are decomposed at different temperatures may simultaneously exist in a porous sample.

The samples studied in this work and in [18] showed two fundamental differences: 1) porous matrix material; 2) water saturation. Paper [18] used silica gel (SiO_2), this work utilised porous Al_2O_3; pore saturation with water in [18] is close to 100 %, while it did not exceed 50 % of maximum in this work (see Fig. 2 and Table 3). We believe that the most probable cause for compliance of the findings acquired by us according to the calculation by method of [18] is low water saturation of the samples used in this work. Indeed, silica gel and alumina surfaces are hydrophilic, hence, the presence of a tightly bound water film between hydrate particles situated in limiting pores and pore walls could be expected in both cases [32]. A hydrate particle contacts only with a layer of tightly bound water, therefore the difference in surface type would have a weak effect on its behaviour.

To assess the effect of water saturation for each of the used samples, the diameter of curvature (D_c) of pores, in which capillary condensation of moisture (see Table 5) takes place, was computed according to formula (3). As demonstrated by comparison of the data of Fig. 1 and Table 2 with the computed values of D_c, the bulk of water in Al_2O_3 samples under study should be located in the domains restricted by the meniscus with surface curvature corresponding to the computed value of D_c. Herewith, inside the domain filled with water, there is quite a large number of small pores completely filled with water. Pores with a size greater than D_c mainly remain unfilled, therefore D_c corresponds to the largest sizes of particles that exist in a porous medium at a specified moisture content. Judging from pore size distribution, it can be considered for our

samples that D_c corresponds to the diameter of the filled pores containing the maximum amount of water.

During hydrate formation in samples with almost 100 % water saturation, the largest amount of pore moisture is present in pores with the D_m diameter corresponding to the maximum on the pore size distribution curve, which appears in experiments with hydrate formation and decomposition [18]. As a whole, it can be assumed that the properties of hydrate generated in the porous structure of silica gel and alumina are similar. There are rather different regularities during examining hydrate formation in natural coal.

Decomposition of methane and carbon dioxide hydrates in pores of natural coals

The gained knowledge on the decomposition of hydrates in the rigid frame of a model for a porous matrix may be useful in examining hydrates formed in natural media of complex composition and irregular pore structure. A significant part of coal seams occur at high pressure, sufficient to form hydrates, and also contains the necessary amount of water and gas.

Each coal grade is characterized by its value of equilibrium moisture content that is set in the atmosphere with a given partial pressure of water vapours. As demonstrated by studies on the formation of carbon dioxide and methane hydrates in the internal structure of coal pores, hydrate is formed in natural coal only when exceeding the threshold value of moisture content [1–6]. However, there was no apparent shift of decomposition points from the equilibrium curve in these experiments [1–6]. Figure 7 demonstrates experimental ranges of decomposition of carbon dioxide hydrate formed in natural coal of G grade collected at the November 7th mine. Coal moisture content was 4.7 %. Experiments were carried out with hydrate decomposition during gas pressure resetting and temperature increasing [4].

The experimental procedure with the decomposition of carbon dioxide and methane hydrates in natural coals is similar to that described above for the degradation of hydrates in a porous alumina matrix [1–3, 5, 6]. Figure 8 gives P–T charts of decomposition of methane hydrates in natural coal [5], occurring in a linear increase in temperature of the coolant surrounding the autoclave. The numbering of the curves in Fig. 8 corresponds to that of experiments carried out with several samples of coal of diverse grades collected at different mines of Kuzbass (Table 6 [5]). Table 6 indicates the specified moisture content (w), the temperature increase rate (Ω), and the amount of water involved in hydrate formation in each experiment (w_h) [5].

In the carried out experiments, moisture content of the samples was only slightly superior to the threshold value typical for each sample of natural coal. There was only one step of methane hydrate decomposition as a bend present near the equilibrium curve in

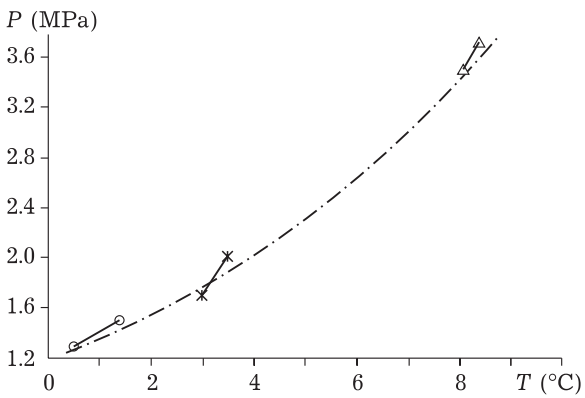

Fig. 7. Decomposition ranges of carbon dioxide hydrate [4] in G grade coal against the equilibrium curve of bulky carbon dioxide hydrate.

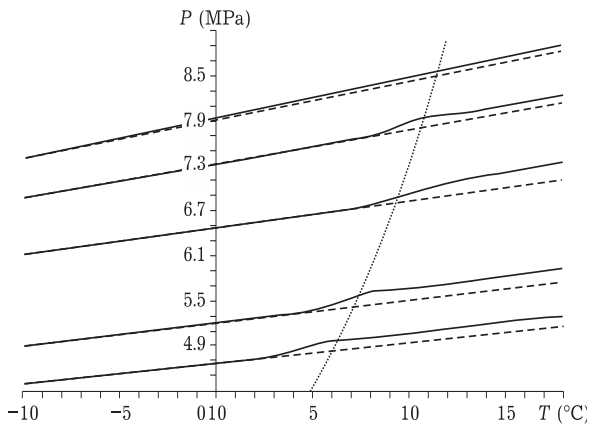

Fig. 8. P–T diagrams of experiments [5] with methane hydrate decomposition in natural coal samples. Points demonstrate the equilibrium curve of methane hydrate; the dash line illustrates the approximation of experimental P–T diagrams.

TABLE 6

Parameters of experiments of methane hydrate decomposition in natural coal samples [5]

Sample number	Mine	Coal grade	w, %	Ω, °C/h	w_h, %
1	Named after Kirov	G	7.56	6.0	0.20
2	Uskovskaya	GF	4.35	4.0	0.50
3	Pervomayskaya	C	2.26	6.0	0.50
4	November 7th	G	4.71	4.5	0.64
5	November 7th	G	4.71	6.0	0.52

all experiments. In experimental procedures described earlier [1–6] and carried out with several samples of coal of different metamorphic grades, decomposition range of methane and carbon dioxide hydrates also almost did not shift from the equilibrium curve. At the same time, the experimental value of shifting decomposition points of the hydrates generate in alumina is 4–13 °C (see Fig. 6). Herein lies the essential difference between the behavior of hydrates formed in natural coal and alumina.

CONCLUSION

Experimental studies have demonstrated an opportunity to generate hydrates from sorbed water and carbon dioxide in the pore space of samples of alumina of three different crystal structures. In accordance with the existing theoretical models, the decomposition temperature of the hydrate generated in the limited pore space is lower than that in bulky hydrated species. The typical sizes of the resulting hydrate particles have been computed on the ground the Gibbs–Thomson equation. When the sorption volume of samples is partially filled with water (about 50 %), the sizes of the produced gas hydrate species are close to the diameter of pores, in which the boundary runs between capillary moisture and gas phase. The presence of two decomposition ranges of hydrate particles could be explained by water drops existence in the pore space of alumina, simultaneously in two forms, *i.e.* spherical and cylindrical. During hydrate destruction in the limited rigid framework of alumina, decomposition points visibly (4–14 °C) deviate from the equilibrium curve, while gas hydrate degradation in coals always proceeds near it. This fact reveals a significant difference in properties of hydrates formed in alumina pores and in the inner space of natural coal.

Acknowledgements

The work was supported by the project No. 18 "Study of physical and chemical properties of hydrate-containing rocks to develop remote methods for detecting and charactersing natural gas hydrate accumulations" of the Complex program of Fundamental Research of SB RAS for 2018.

REFERENCES

1 Smirnov V. G., Manakov A. Yu., Ukraintseva E. A., Villevald G. V., Karpova T. D., Dyrdin V. V., Lyrshchikov S. Yu., Ismagilov Z. R., Terekhova I. S., Ogienko A. G., *Fuel*, 2016, Vol. 166, P. 188–195.

2 Smirnov V. G., Manakov A. Yu., Dyrdin V. V., Ismagilov Z. R., *Vestnik Kuzbasskogo Gosudarstvennogo Tekhnicheskogo Universiteta*, 2014, No. 2 (102), P. 27–30.

3 Smirnov V. G., Manakov A. Yu., Dyrdin V. V., *Vestnik Kuzbasskogo Gosudarstvennogo Tekhnicheskogo Universiteta*, 2014, No. 3 (103), P. 24–28.

4 Dyrdin V. V., Smirnov V. G., Kim T. L., Manakov A. Yu., Fofanov A. A., Kartopolova I. S., *Rus. Phys. J.*, 2017, Vol. 60, No. 2, P. 206–214.

5 Smirnov V. G., Dyrdin V. V., Manakov A. Yu., Ismagilov Z. R., Adamova T. P., *Khimiya Ust. Razv.*, 2016, Vol. 24, No. 4, P. 499–507.

6 Smirnov V. G., Dyrdin V. V., Ismagilov Z. R., Kim T. L., Manakov A. Yu., *Vestnik Nauchnogo Tsentra po Bezopasnosti Rabot v Ugol'noj Promyshlennosti*, 2017, No. 1, P. 34–41.

7 Smirnov V. G., Dyrdin V. V., Ismagilov Z. R., Kim T. L., *Izvestiya Vysshikh Uchebnykh Zavedenij. GORNYJ Zhurnal*, 2016, No. 3, P. 96–103.

8 Makogon Yu. F., Morozov I. F., *Bezopasnost' Truda v Promyshlennosti*, 1973, No. 12, P. 36–37.

9 Dyrdin V. V., Smirnov V. G., Shepeleva S. A., *J. Min. Sci.*, 2013, Vol. 49 (6), P. 908–12.

10 Smirnov V. G., Manakov A. Yu., Dyrdin V. V., Khitsova L. M., Mikhailova E. S., Ismagilov Z. R., *Koks i Khimiya*, 2017, No. 10, P. 2–7.

11 Ismagilov Z. R., Shikina N. V., Zhuravleva N. V., Potokina

R. R., Teryaeva T. N., Kerzhentsev M. A., *Khimiya Tverdogo Topliva*, 2014, No. 4, P. 3–11.
12 Fedorova N. I., Khitsova L. M., Malysheva V. Yu., Ismagilov Z. R., Zhuravleva N. V., Potokina R. R., *Khimiya Ust. Razv.*, 2015, Vol. 23, No. 4, P. 433–438.
13 Shikina N. V., Khabibullina E. R., Mikhailova E. S., Zhuravleva N. V., Ismagilov Z. R., *Koks i Khimiya*, 2017, Vol. 9, P. 18–25.
14 Sloan E. D., Koh C. A. Clathrate Hydrates of Natural Gases, 3d Ed., Boca Rator–London–NY, CRC Press, 2008.
15 Kuznetsov F. A., Istomin V. A., Rodionova T. V., *Rossijskij Khimicheskij Zhurnal (Zhurn. Ros. Khim. Obshchestva Im. D. I. Mendeleeva)*, 2003, Vol. XLVII, No. 3, P. 5–18.
16 Koryakina V. V., Ivanova I. K., Shits E. Yu., *Khimiya Ust. Razv.*, 2017, Vol. 25, No. 6, P. 633–638.
17 Istomin V. A., Yakushev V. S., Gazovye Gidraty v Pripodnykh Usloniyakh, Moskva, Nedra, 1992. 236 p.
18 Aladko E. Ya., Dyadin Yu. A., Fenelonov V. B., Larionov E. G., Manakov A. Yu., Mel'gunov M. S., Zhurko F. V., *J. Phys. Chem. B.*, 2006, Vol. 110, P. 19717–19725.
19 Christenson H. K., *J. Phys. Condens. Matter.*, 2001, Vol. 13, R95.
20 Alba-Simionesko C., Coasne B., Dudziak G., Gubbins K. E., *J. Phys. Condens. Matter.*, 2006, Vol. 18, R15–R68.
21 Turner D. J., Cherry R. S., Sloan E. D., *Fluid Phase Equilibria*, 2005, Vol. 228–229, P. 505–510.
22 Anderson R., Llamedo M., Tohidi B., Burgass R. W., *J. Phys. Chem. B*, 2003, Vol. 107, P. 3507–3514.
23 Ismagilov Z. R., Kerzhentsev M. A., *Catal. Rev. Sci. Eng.*, 1990, Vol. 32 (1–2), P. 51–103.
24 Boreskov G. K., Levitskii E. A., Ismagilov Z. R., *J. All-Union Mendeleev Chem. Soc.*, 1984, Vol. 29 (4), P. 379–385.
25 Ismagilov Z. R., Shkrabina R. A., Koryabkina N. A., Kapteijn F., *Catal. Today*, 1995, Vol. 24 (3), P. 269–271.
26 Ismagilov Z. R., Shkrabina R. A., Kirchanov A. A., Koryabkina N. A., Pex P., Veringa H., *Reaction Kinet. Catal. Lett.*, 1997, Vol. 60, P. 225–231.
27 Ismagilov Z. R., Shepeleva M. N., Shkrabina R. A., Fenelonov V. B., *Appl. Catal.*, 1991, Vol. 69, P. 65–73.
28 Shepeleva M. N., Shkrabina R. A., Fenelonov V. B., Ismagilov Z. R., *Appl. Catal.*, 1991, Vol. 78, P. 175–184.
29 Ismagilov Z. R., Shkrabina R. A., Koryabkina N. A., *Catal. Today*, 1999, Vol. 47, P. 51–71.
30 Rid R., Prausnits Dzh., Shervud T. Svojstva Gazov i Zhidkostej. Sprav. Posobie, Leningrad, Khimiya, 1982. 592 p.
31 Circone S., Stern L. A., Kirby S. H., Durham W. B., Chakoumakos B. C., Rawn C. J., Rondinone A. J., Ishii Y., *J. Phys. Chem. B*, 2003, Vol. 107, P. 5529–5539.
32 Fenelonov V. B., Vvedenie v Fizicheskuyu Khimiyu Formirovaniya Supramolekulyarnoj Struktury Adsorbentov i Katalizatorov, Novosibirsk, Izd-vo SO RAN, 2004. 442 p